Inorganic Chemistry

Article

pubs.acs.org/IC

Titanium/Yttrium Mixed Metal Nitride Clusterfullerene $TiY_2N@C_{80}$: Synthesis, Isolation, and Effect of the Group-III Metal

Chuanbao Chen,[†] Fupin Liu,[†] Shujuan Li,[‡] Nan Wang,[†] Alexey A. Popov,[§] Mingzhi Jiao,[†] Tao Wei,[†] Qunxiang Li,[‡] Lothar Dunsch,[§] and Shangfeng Yang*[,†]

[†]Hefei National Laboratory for Physical Sciences at Microscale, CAS Key Laboratory of Materials for Energy Conversion & Department of Materials Science and Engineering, University of Science and Technology of China (USTC), Hefei 230026, China

[‡]Hefei National Laboratory for Physical Sciences at Microscale & Department of Chemical Physics, University of Science and Technology of China (USTC), Hefei 230026, China

[§]Center of Spectroelectrochemsitry, Department of Electrochemistry and Conducting Polymers, Leibniz-Institute for Solid State and Materials Research (IFW) Dresden, D-01171 Dresden, Germany

Supporting Information

ABSTRACT: Titanium/yttrium mixed metal nitride clusterfullerene (MMNCF) $TiY_2N@C_{80}$ has been successfully synthesized, representing the first Ti-containing non-scandium MMNCF. $TiY_2N@C_{80}$ has been isolated by multistep HPLC and characterized by various spectroscopies in combination with DFT computations. The electronic absorption property of $TiY_2N@C_{80}$ was characterized by UV−vis−NIR spectroscopy, indicating the resemblance to that of $TiSc_2N@C_{80}$ with broad shoulder absorptions. The optical band gap of $TiY_2N@C_{80}$ (1.39 eV) is very close to that of $TiSc_2N@C_{80}$ (1.43 eV) but much smaller than that of $Y_3N@C_{80}$ (I_h, 1.58 eV). Such a resemblance of the overall absorption feature of $TiY_2N@C_{80}$ to $TiSc_2N@C_{80}$ suggests that $TiY_2N@C_{80}$ has a similar electronic configuration to that of $TiSc_2N@C_{80}$, that is, $(TiY_2N)^{6+}@C_{80}^{6-}$. FTIR spectroscopic study and DFT calculations accomplish the assignment of the C_{80}:I_h isomer to the cage structure of $TiY_2N@C_{80}$, with the C_1 conformer being the lowest energy structure, which is different from the C_s conformer assigned to $TiSc_2N@C_{80}$. The electrochemical properties of $TiY_2N@C_{80}$ were investigated by cyclic voltammetry, revealing the reversible first oxidation and first reduction step with $E_{1/2}$ at 0.00 and −1.13 V, respectively, both of which are more negative than those of $TiSc_2N@C_{80}$, while the electrochemical energy gap of $TiY_2N@C_{80}$ (1.11 V) is almost the same as that of $TiSc_2N@C_{80}$ (1.10 V). Contrary to the reversible first reduction step, the second and third reduction steps of $TiY_2N@C_{80}$ are irreversible, and this redox behavior is dramatically different from that of $TiSc_2N@C_{80}$, which shows three reversible reduction steps, indicating the strong influence of the encaged group-III metal (Y or Sc) on the electronic properties of $TiM_2N@C_{80}$ (M = Y, Sc).

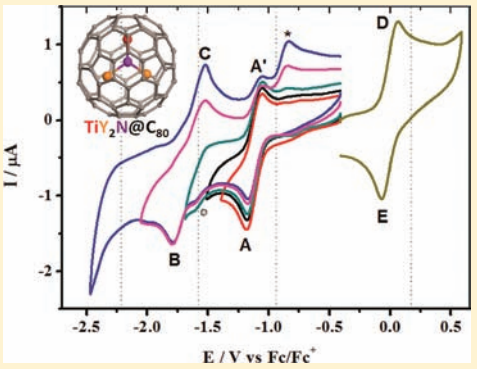

INTRODUCTION

As a special class of endohedral fullerenes, metal nitride clusterfullerenes (NCFs) show unique electronic, physical, and chemical properties arising from encapsulation of trimetallic nitride cluster within the carbon cage.[1−4] Mixed metal nitride clusterfullerenes (MMNCFs) represent a branch family of NCFs with two or three different metals mixed in the encaged nitride cluster.[1,4−16] Because of the highest yield of scandium (Sc)-based NCFs as compared to homogeneous NCFs with other metals,[1] comprehensive studies on Sc-based MMNCFs ($M_xSc_{3-x}N@C_{2n}$), including $M_xSc_{3-x}N@C_{80}$ (M = Y,[5] Ce,[6] Nd,[7] Gd,[8,9] Tb,[10] Dy,[11] Er,[2,5,12] Lu[7]), $DySc_2N@C_{76}$,[11] $Lu_2ScN@C_{68}$, $MSc_2N@C_{68}$ (M = Dy, Lu),[13] reveal that Sc can direct formation of the MMNCFs.[4] As a result, for the synthesis of $M_xSc_{3-x}N@C_{2n}$, the yield of the homogeneous Sc−NCFs generally dominates that of the M-based homogeneous NCFs for which formation is dramatically suppressed.[4] In contrast, non-Sc MMNCFs, i.e., MMNCFs without the involvement of Sc ($L_xM_{3-x}N@C_{2n}$), appear more intriguing because the possible competition between two different metals (L, M) comprising of the mixed metal nitride may complicate not only the relative yield of the homogeneous NCFs based on the two different metals but also the structure of the MMNCFs. Thusfar only two types of non-Sc MMNCFs have been isolated, including $Lu_xY_{3-x}N@C_{80}$[14] and $Lu_2CeN@C_{80}$.[15] Compared to $Lu_xSc_{3-x}N@C_{80}$, within $Lu_xY_{3-x}N@C_{80}$ the relatively larger Y metal atoms move to the centers of the hexagons of the carbon cage, and this leads to the increase of the pyramidalization of the pyrene-type carbon atoms.[14] $Lu_2CeN@C_{80}$ exhibits an unprecedented oxidation behavior via removal of the Ce-4f electron bypassing the carbon cage, whereas in all other $M_3N@C_{80}$ (M = Sc, Y, lanthanides) NCFs the cage electron is removed upon oxidation.[15] MMNCFs

Received: October 31, 2011
Published: February 10, 2012

   dx.doi.org/10.1021/ic202354u | Inorg. Chem. 2012, 51, 3039−3045

$L_xM_{3-x}N@C_{2n}$ appear quite peculiar because not only their yield (e.g., $MSc_2N@C_{80}$) could be even higher than that of the homogeneous NCFs (e.g., $Sc_3N@C_{80}$) but also the structure variation may be easily achieved by tuning the composition of the mixed-metal nitride (e.g., x value).[4,8,9,14]

Recently we successfully synthesized and isolated a Ti/Sc MMNCF, $TiSc_2N@C_{80}$, which represents the first success of encapsulating a non-group-III metal into NCFs.[16,17] FTIR spectroscopic study in combination with DFT calculation accomplishes the assignment of the C_{80}:I_h isomer to the cage structure of $TiSc_2N@C_{80}$.[16] By studying the role of the Ti atom in $TiSc_2N@C_{80}$ as compared to $Sc_3N@C_{80}$, we found that the redox behavior of $TiSc_2N@C_{80}$ differed markedly from those of homogeneous $M_3N@C_{80}$ NCFs in giving reversible one-electron transfers even on the cathodic scale. The unpaired electron spin in $TiSc_2N@C_{80}$ was found to be preferably fixed at the Ti ion as shown by low-temperature ESR measurements and confirmed by DFT calculations.[17] Given that so far only $TiSc_2N@C_{80}$ was reported as the Ti-containing NCF and substitution of one Sc atom within $Sc_3N@C_{80}$ by Ti atom results in a dramatic change of the electronic structure, two open questions worth addressing are whether the Ti atom could be encapsulated in another type of NCF, especially non-Sc NCF, and consequently how Ti and group-III metal would affect the structure and properties of NCF.

In this paper, we report on the synthesis and isolation of $TiY_2N@C_{80}$ as the first Ti-containing non-Sc MMNCF. The electronic property of $TiY_2N@C_{80}$ was characterized by UV−vis−NIR, XPS, and ESR spectroscopies and cyclic voltammetry. The vibrational structure of $TiY_2N@C_{80}$ was studied by FTIR. In combination with DFT calculations, the cage structure of $TiY_2N@C_{80}$ was determined. On the basis of the comparative study on the elution behavior and electronic property between $TiY_2N@C_{80}$ and $TiSc_2N@C_{80}$, the influence of the group-III metal on the structure and properties of Ti-based MMNCFs $TiM_2N@C_{80}$ (M = Y, Sc) was addressed.

RESULTS AND DISCUSSION

Synthesis and Isolation of $TiY_2N@C_{80}$. $TiY_2N@C_{80}$ was synthesized by a modified Krätschmer−Huffman method using an equimolar mixture of TiO_2 and Y_2O_3 as the raw material with addition of ~2.5% N_2, which is similar to that used for synthesis of $TiSc_2N@C_{80}$.[16] Figure 1 shows the typical chromatogram of the TiO_2/Y_2O_3 extract mixture (curve a), which also includes those obtained from pure Y_2O_3 (curve b) and TiO_2/Sc_2O_3 (curve c) for comparison. Obviously the HPLC profile of the TiO_2/Y_2O_3 extract differs from that of the pure Y_2O_3 extract at t_{ret} > 20.5 min (see inset of Figure 1), and their major difference is found for fraction **A** (t_{ret} = 20.8−23.3 min), for which the center of the HPLC peak of the TiO_2/Y_2O_3 extract (t_{ret} = 22.1 min) shifts positively compared to that of the pure Y_2O_3 extract (t_{ret} = 21.5 min). Since the HPLC conditions used for analysis of these extracts are exactly same, such a shift must be due to the variation of the composition of fraction **A**.

To check the composition of fraction **A**, laser desorption time-of-flight (LD-TOF) MS analysis was carried out, indicating the dramatic difference between fraction **A** of the TiO_2/Y_2O_3 and the pure Y_2O_3 extracts: the most intense mass peak detected at m/z = 1241 ($Y_3N@C_{80}$) for the pure Y_2O_3 extracts becomes very weak in that of the TiO_2/Y_2O_3 extract; instead, a new and intense mass peak at m/z = 1200 appears (Figure S1, Supporting Information). Clearly, this new mass peak at m/z = 1200 is absent in the mass spectrum of the pure

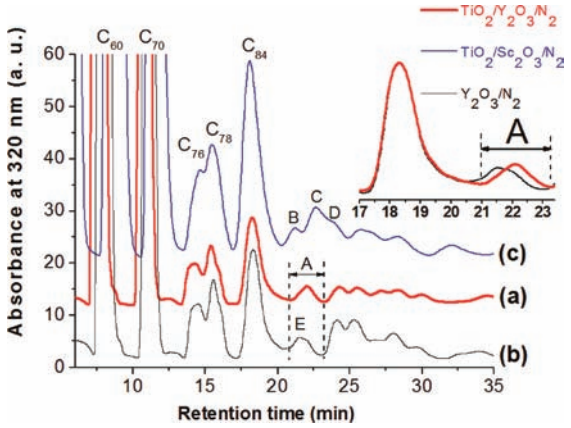

Figure 1. Chromatograms of the fullerene extract mixtures synthesized from TiO_2/Y_2O_3 (a), pure Y_2O_3 (b), and and TiO_2/Sc_2O_3 (c) (20 × 250 mm 5PYE column; flow rate 15.0 mL/min; injection volume 15 mL; toluene as eluent; 25 °C). Fractions **B**, **C**, and **D** of TiO_2/Sc_2O_3 extract contain mainly $Sc_3N@C_{78}$, $Sc_3N@C_{80}$ (I_h), and $Sc_3N@C_{80}$ (D_{5h}) + $TiSc_2N@C_{80}$, respectively.[16] Fraction **E** of pure Y_2O_3 extract contains mainly $Y_3N@C_{80}$ (I_h). The slight shifts of the retention times of C_{60} and C_{70} are due to the temperature fluctuation of the column. (Inset) Enlarged chromatographic region of 17−23.5 min containing fraction **A**.

Y_2O_3 extract, suggesting that this new mass peak is due to formation of Ti-containing NCFs, which is likely $TiY_2N@C_{80}$.

Fraction **A** was isolated by two-step HPLC (see Figure S2, Supporting Information, for the detailed isolation procedure). Briefly, in the first-step HPLC isolation running on a 5PYE column (Figure S2I, Supporting Information) fraction **A-3** was found to contain the new structure with a mass peak at m/z = 1200 according to LD-TOF MS analysis and collected for second-step HPLC isolation running on a Buckyprep-M column, resulting in successful isolation of fraction **A-3-3**, which shows a single mass peak at m/z = 1200 as confirmed by LD-TOF MS analysis (see Figure 2II). The purity of the

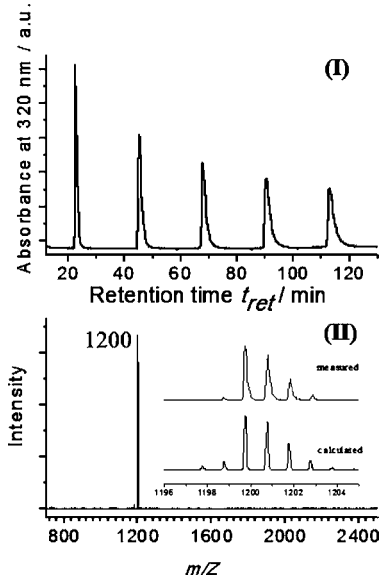

Figure 2. (I) Chromatogram of isolated $TiY_2N@C_{80}$ (10 × 250 mm Buckyprep-M column; flow rate 5.0 mL/min; injection volume 5 mL; toluene as eluent; 25 °C). (II) Positive-ion laser desorption time-of-flight (LD-TOF) mass spectrum of $TiY_2N@C_{80}$. (Insets) Measured and calculated isotope distributions of $TiY_2N@C_{80}$.

dx.doi.org/10.1021/ic202354u | Inorg. Chem. 2012, 51, 3039−3045

isolated fraction **A-3-3** (ca. 10 mg) was further checked by recycling HPLC (Figure 2I). The single peak observed in the HPLC profile of the product even after four cycles indicates its high purity. Chemical identification of the proposed new fullerene structure, $TiY_2N@C_{80}$, is also accomplished by isotopic distribution analysis of the mass peak at 1200, which shows a good coincidence with the calculated one (see inset of Figure 2II).

Compared to the HPLC profile of TiO_2/Sc_2O_3 extract (curve c),[16] for the TiO_2/Y_2O_3 extract (curve a) the intensities of the major HPLC peaks including the NCFs (t_{ret} > 20.5 min) and empty fullerenes such as C_{76}, C_{78}, and C_{84}, etc., are obviously lower, indicating the decrease of their absolute yield. Specifically, for the major NCFs of TiO_2/Sc_2O_3 extract (fractions **B**, **C**, and **D**, $Sc_3N@C_{78}$, $Sc_3N@C_{80}$ (I), $Sc_3N@C_{80}$ (II), and $TiSc_2N@C_{80}$, respectively),[16] their absolute yield is evidently higher than those of TiO_2/Y_2O_3 extract (fraction **A**). This is mainly due to the lower yield of $Y_3N@C_{80}$ compared to $Sc_3N@C_{80}$, as already revealed for the homogeneous NCFs based on Y and Sc.[1,5] Interestingly, while $TiSc_2N@C_{80}$ was isolated from fraction **D** of the TiO_2/Sc_2O_3 extract as a shoulder peak of fraction **C** and its retention time (t_{ret}) is obviously larger than that of $Sc_3N@C_{80}$ (I) (fraction **C**),[16] $TiY_2N@C_{80}$ was co-eluted with $Y_3N@C_{80}$ within fraction **A** of the TiO_2/Y_2O_3 extract, indicating that t_{ret} of $TiY_2N@C_{80}$ is close to that of $Y_3N@C_{80}$, which are both smaller than those of $Sc_3N@C_{80}$ and $TiSc_2N@C_{80}$ (see curves a and c). Since t_{ret} is determined by the intermolecular interactions between fullerenes and the stationary phase of the 5PYE column (2-(1-pyrenyl)ethyl group),[1] the close t_{ret} of $TiY_2N@C_{80}$ and $Y_3N@C_{80}$ suggests their similarity on the interactions with the 2-(1-pyrenyl)ethyl group, whereas the difference between $TiSc_2N@C_{80}$ and $Sc_3N@C_{80}$ seems larger. Given that the ionic radius of Ti^{3+} (0.67 Å) is actually closer to that of Sc^{3+} (0.75 Å) and much smaller than that of Y^{3+} (0.90 Å),[16,18,19] these results reveal that the elution behavior of Ti-containing MMNCFs $TiM_2N@C_{80}$ (M = Y, Sc) is not a simple size effect but dependent strongly on the nature of the group-III metal.

It should be noted that under our synthesis conditions only one type of Ti-containing MMNCF ($TiY_2N@C_{80}$) was detected in the LD-TOF MS in fraction **A**, which is very similar to the case of TiO_2/Sc_2O_3 extract.[16] This indicates the clear difference of Ti/Y MMNCFs to those reported $M_xSc_{3-x}N@C_{80}$ fullerenes (M is a group-III metal) or other non-scandium MMNCFs ($L_xM_{3-x}N@C_{80}$) for which two compositions of the mixed-metal nitride (LM_2N or L_2MN, x = 1 or 2) as well as two isomers of $M_xSc_{3-x}N@C_{80}$ are generally formed.[1,4−16]

Spectroscopic Studies of the Electronic Structure of $TiY_2N@C_{80}$. Figure 3 presents the UV−vis−NIR spectrum of the isolated $TiY_2N@C_{80}$ dissolved in toluene (curve a, see also Figure S3, Supporting Information) in comparison with those of $TiSc_2N@C_{80}$ (curve b) and $Y_3N@C_{80}$ (I, I_h) (curve c). Obviously the UV−vis−NIR spectrum of $TiY_2N@C_{80}$ shows a higher resemblance to that of $TiSc_2N@C_{80}$, both exhibiting broad shoulder absorptions.[16] Compared to the UV−vis−NIR spectrum of $Y_3N@C_{80}$ (I, I_h) with several distinct absorption peaks at 407, 549, 633, 665, and 694 nm,[14] that of $TiY_2N@C_{80}$ is less rich in features and the four broad shoulder absorption peaks observed for $TiY_2N@C_{80}$ (405, 541, 641, and 708 nm) seem to be correlated with those in the absorption spectrum of $Y_3N@C_{80}$ (I, I_h) but exhibit detectable shifts (see inset of Figure 3).[14]

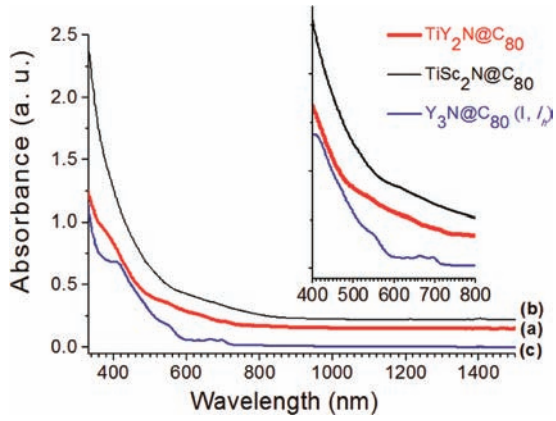

Figure 3. UV−vis−NIR spectrum of $TiY_2N@C_{80}$ dissolved in toluene (a) in comparison with those of $TiSc_2N@C_{80}$ (b) and $Y_3N@C_{80}$ (I, I_h, c). Spectra of $TiY_2N@C_{80}$ and $TiSc_2N@C_{80}$ are shifted vertically for clarity. (Inset) Enlarged spectral range (400−800 nm).

Noteworthy, the estimated optical band gap of $TiY_2N@C_{80}$ (1.39 eV) based on the absorption spectral onset of ca. 890 nm is also quite close to that of $TiSc_2N@C_{80}$ (1.43 eV) but much smaller than that of $Y_3N@C_{80}$ (I, I_h, 1.58 eV).[14,16] It is known that the electronic absorptions of fullerenes are predominantly due to $\pi-\pi^*$ carbon cage excitations and depend on the structure and charge state of the carbon cage.[1,4] Therefore, the resemblance of the overall absorption feature of $TiY_2N@C_{80}$ to $TiSc_2N@C_{80}$ suggests that $TiY_2N@C_{80}$ has a similar electronic configuration to that of $TiSc_2N@C_{80}$, that is, $(TiY_2N)^{6+}@C_{80}^{6-}$.[16,17] Accordingly, the formal electronic state of Ti^{3+} is expected for Ti, which is further confirmed by the X-ray photoemission spectroscopy (XPS) study (see Figure S4, Supporting Information). The encaged Ti $2p_{3/2}$ and $2p_{1/2}$ binding energies in $TiY_2N@C_{80}$ are 455.8 and 461.7 eV (Figure S4, Supporting Information), respectively, which is very close to that in $TiSc_2N@C_{80}$ (455.7 and 461.3 eV),[16] suggesting that the valence state of Ti is 3.

Taking the electronic configuration of $(TiY_2N)^{6+}@C_{80}^{6-}$ with the formal electronic state of Ti^{3+} into account, $TiY_2N@C_{80}$ should be paramagnetic due to localization of one unpaired electron on Ti^{3+} ($3d^1$). This inference was confirmed by the lack of ^{13}C NMR signal after spectrum accumulation for 7 days and further by detection of the evident ESR signals even at room temperature, indicating that the broad signal with a g factor of 1.9579 detected at room temperature becomes more intense and sharper with the decrease of the measurement temperature down to 200 K (Figure 4). ESR measurements show that $TiY_2N@C_{80}$ is a radical with significant anisotropy of the g tensor. Interestingly, compared to the ESR spectrum of $TiSc_2N@C_{80}$, which exhibits a broad signal with a g factor of 1.9454 (room-temperature condition),[16,17] the line width of the ESR lines of $TiY_2N@C_{80}$ is much smaller than that of $TiSc_2N@C_{80}$ (see Table S2, Supporting Information), indicating that these two Ti-based MMNCFs have different electronic structures, which presumably attribute to the difference on the spin distribution of the two TiM_2N clusters resulting from the different electronic configurations between Y^{3+} and Sc^{3+} as well as the different geometric structures of TiM_2N. According to our DFT calculations as discussed below, the bond length of Y−N within $TiY_2N@C_{80}$ is larger than that of Sc−N within $TiSc_2N@C_{80}$ while the bond length of Ti−N within $TiY_2N@C_{80}$ is smaller than that within $TiSc_2N@C_{80}$ (see Table 1).

dx.doi.org/10.1021/ic202354u | Inorg. Chem. 2012, 51, 3039−3045

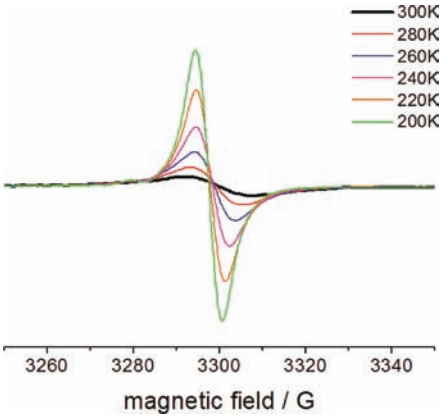

Figure 4. ESR spectra of $TiY_2N@C_{80}$ in toluene measured under different temperatures.

Table 1. Selected DFT-Predicted Bond Lengths (Angstroms) of $TiY_2N@C_{80}$ in Comparison with Those of $TiSc_2N@C_{80}$ and $Y_3N@C_{80}$ (I_h)[14,16,17]

bond length (Å)	$TiY_2N@C_{80}$	$TiSc_2N@C_{80}$	$Y_3N@C_{80}$
d(Y–N)	2.140/2.147		2.051/2.052
d(Sc–N)		2.007	
d(Ti–N)	1.846	1.921	
d(Y–C)	2.390		2.373
d(Sc–C)		2.255	
d(Ti–C)	2.165	2.214	
d(Y–Y)	3.672		3.552/3.555
d(Sc–Sc)		3.596	
d(M–Ti)	3.547/3.399	3.460/3.458	

Molecular and Vibrational Structures of $TiY_2N@C_{80}$. The FTIR spectrum of $TiY_2N@C_{80}$ (curve a) in comparison with those of $Y_3N@C_{80}$ (I, I_h) (curve b) and $TiSc_2N@C_{80}$ (curve d) are shown in Figure 5. The radial cage vibrational modes of $TiY_2N@C_{80}$ and $Y_3N@C_{80}$ (around 490 cm^{-1}) are completely identical, while the tangential modes of $TiY_2N@C_{80}$ (region of 1100–1600 cm^{-1}) with four main bands (cm^{-1}) at 1380, 1461, 1493, and 1532 cm^{-1} are quite close to those of $Y_3N@C_{80}$ (I, I_h, 1376, 1461, 1493, and 1516 cm^{-1}), suggesting the same cage isomeric structure of the two NCFs, that is, C_{80}:I_h(7).[14] The cage tangential modes of $TiY_2N@C_{80}$ are also similar to those of $TiSc_2N@C_{80}$, for which the main bands are observed at 1204, 1367, 1450, and 1519 cm^{-1}.[16]

The dramatic difference between the FTIR spectra of these three NCFs was observed in the region of 600–800 cm^{-1}, which is assigned as the antisymmetric M–N stretching vibration (ν_{M-N}).[1,4,19] As revealed in our previous studies of $M_xSc_{3-x}N@C_{80}$ (M = Y, Ce, Gd, Tb, Dy, Er, Lu)[4,7–9] and $Lu_xY_{3-x}N@C_{80}$,[14] MMNCFs generally show the splitting of ν_{M-N} because of the lower cluster symmetry; this is quite different than the homogeneous NCFs in which ν_{M-N} is 2-fold degenerated.[1,4,19] For $TiY_2N@C_{80}$, it is found that these modes (ν_{Y-N} and ν_{Ti-N}) experience a similar splitting with four main bands observed at 791, 725, 709, and 695 cm^{-1}. On the contrary, ν_{Y-N} within $Y_3N@C_{80}$ are observed at 725, 714, and 698 cm^{-1}.[14] A similar phenomena was also found for $TiSc_2N@C_{80}$ at 504 and 606 cm^{-1} for ν_{Sc-N} and ν_{Ti-N}, respectively, whereas ν_{Sc-N} of $Sc_3N@C_{80}$ (I, I_h) was detected at 599 cm^{-1}.[16]

In order to study the cage isomeric structure and assign the vibrational modes, we performed spin-polarized DFT computations considering several possible conformers of $TiY_2N@C_{80}$ as well as $TiSc_2N@C_{80}$.[20,21] Figure 6a illustrates the DFT-optimized structure of the lowest energy conformers of $TiY_2N@C_{80}$ with C_{80}:I_h cage. Our previous DFT study on $TiSc_2N@C_{80}$ revealed that the C_s conformer of $TiSc_2N@C_{80}$

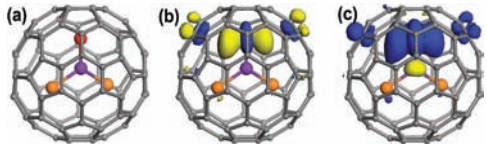

Figure 6. (a) Optimized molecular structure of the lowest energy conformer of $TiY_2N@C_{80}$ (C_1) at the PBE-GGA/DNP level. (b) Spatial distribution of the HOMO of the spin-up state. (c) Spin density of the most stable conformer (C_1) of $TiY_2N@C_{80}$. Ti, Y, and N atoms are drawn in red, orange, and purple, respectively.

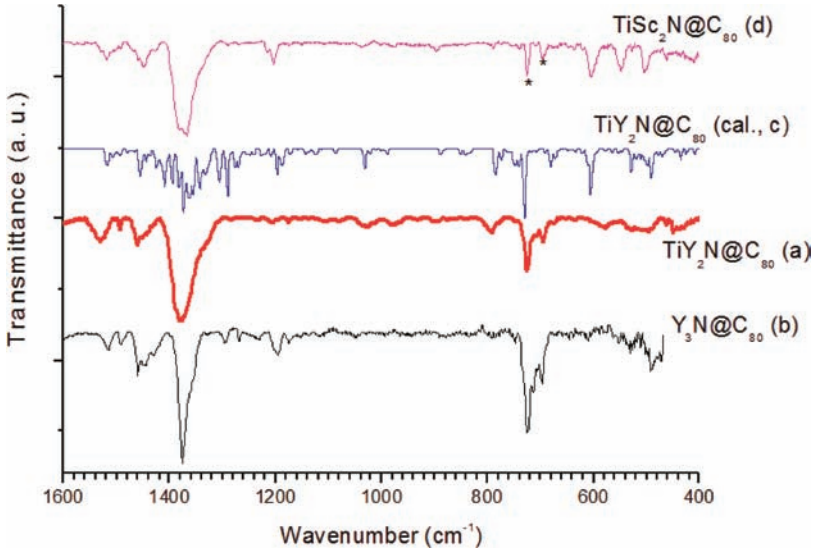

Figure 5. FTIR spectra of $TiY_2N@C_{80}$ (a), $Y_3N@C_{80}$ (I, I_h, b), and $TiSc_2N@C_{80}$ (d, ref 16). Asterisks in curve d label the toluene lines which could not be removed after heating. DFT-simulated IR spectrum of $TiY_2N@C_{80}$ (I_h, c) is also shown for comparison.

dx.doi.org/10.1021/ic202354u | Inorg. Chem. 2012, 51, 3039–3045

has the lowest energy and the conformers of $TiSc_2N@C_{80}$ derived from the C_{3v} and C_s conformers of $Sc_3N@C_{80}$ are isoenergetic within 1 kJ·mol^{-1} and are more stable than that derived from the C_3 conformer of $Sc_3N@C_{80}$ (by 13 kJ·mol^{-1}).[16,17] Similarly, for $TiY_2N@C_{80}$, our DFT study reveals that the C_1 conformer has the lowest energy, which is different from that of $TiSc_2N@C_{80}$ (C_s conformer).[20] These results suggest that the cage isomeric structure of Ti-based MMNCFs $TiM_2N@C_{80}$ (M = Y, Sc) is sensitively dependent on the encaged group-III metal (Y or Sc). Actually, according to our analysis of the spin-polarized Kohn–Sham molecular orbital and the partial density of states, we find that the $TiY_2N@C_{80}$ molecule displays magnetism and the molecular magnetic moment (MM) is predicted to be about 0.86 μ_B. Figure 6b shows the spatial distribution of the highest occupied molecular orbital (HOMO) of the spin-up state, which is largely localized around the Ti atom. This indicates that the molecular MM is mainly contributed by the unpaired 3d electron of the Ti atom. The spin density of $TiY_2N@C_{80}$ is plotted in Figure 6c. Clearly, the spin density is mostly localized on the encapsulated TiY_2N cluster and in particular on the Ti atom. The net spin population of the whole encapsulated cluster is up to 0.98, which is mainly dominated by the Ti atom (about 0.85), the N atom has a small negative spin population (−0.06), and two Y atoms give negligible contributions. Noteworthy, all of these features are similar to those of $TiSc_2N@C_{80}$.[16,17]

To reveal the structural difference between $TiY_2N@C_{80}$ and $TiSc_2N@C_{80}$ we also optimized the geometric parameters for $TiM_2N@C_{80}$ at the same level of theory. Table 1 compares the bond-length parameters of $TiY_2N@C_{80}$ and $TiSc_2N@C_{80}$. Although both MMNCFs show a substantial resemblance, the Y–N bonds in $TiY_2N@C_{80}$ (2.140/2.147 Å) are longer than those of Sc–N in $TiSc_2N@C_{80}$ (2.007 Å). On the contrary, the Ti–N bond in $TiY_2N@C_{80}$ becomes much shorter (1.846 Å) compared to that in $TiSc_2N@C_{80}$ (1.921 Å), suggesting that the N atom moves closer to the Ti atom within the TiY_2N cluster compared to that within $TiSc_2N$ cluster.

The determined cage isomeric structure of $TiY_2N@C_{80}$ (C_{80}:I_h) was confirmed by comparing its experimental FTIR spectrum (curve a, Figure 5) and the DFT-simulated IR spectrum of $TiY_2N@C_{80}$ (I_h) (curve c, Figure 5), illustrating a reasonable agreement of these two spectra in the ranges of both the tangential and the radial cage modes. This result solidifies the above assignment of the cage structure of $TiSc_2N@C_{80}$ (I_h). According to DFT calculations, the antisymmetric Ti–N stretching vibrational band (ν_{Ti-N}) is predicted to be 731 cm^{-1}, which is observed at 725 cm^{-1} in the experimental spectrum. Obviously ν_{Ti-N} within $TiY_2N@C_{80}$ is much higher than that within $TiSc_2N@C_{80}$ (606 cm^{-1}).[16,17] This difference originates from the different Ti–N bond length in these two MMNCFs as discussed above (see Table 1).

The assignment of C_{80}:I_h to the cage structure of $TiY_2N@C_{80}$ was further supported by the similarity of the elution behavior and UV–vis–NIR and FTIR spectra between $TiY_2N@C_{80}$ and the analogous $Y_3N@C_{80}$ (I_h) for which the cage structure had been unambiguously determined by X-ray crystallography.[22,23] As discussed above, the retention time (t_{ret}) of $TiY_2N@C_{80}$ is close to that of $Y_3N@C_{80}$ (I_h) (see curve a of Figure 1), suggesting their similarity on the interactions with the 2-(1-pyrenyl)ethyl group as the stationary phase of the 5PYE column. Since t_{ret} is strongly dependent on the cage symmetry for the $M_xSc_{3-x}N@C_{80}$ MMNCFs,[7−9] the close t_{ret} of $TiY_2N@C_{80}$ to that of $Y_3N@C_{80}$ (I_h) is obviously resulting from their similarity on the cage symmetry (C_{80}:I_h). Moreover, the UV–vis–NIR and FTIR spectra of $TiY_2N@C_{80}$ exhibit high resemblance to those of $Y_3N@C_{80}$ (I_h) as well, confirming further their similarity on the cage symmetry of C_{80}:I_h.

Electrochemical Study of $TiY_2N@C_{80}$. The cyclic voltammogram of $TiY_2N@C_{80}$ measured in *o*-DCB solution with $TBAPF_6$ as supporting electrolyte is presented in Figure 7,

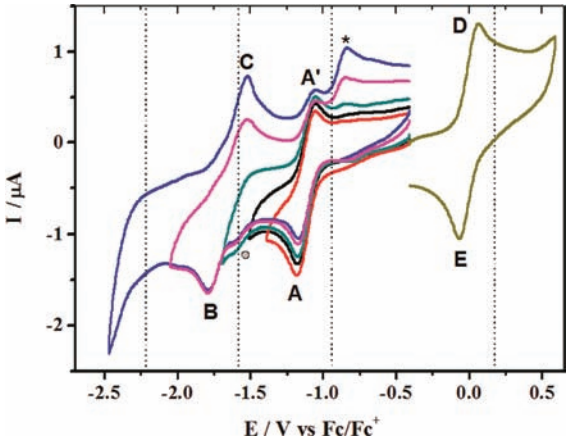

Figure 7. Cyclic voltammogram of $TiY_2N@C_{80}$ in *o*-DCB solution under different scan regions. Ferrocene (Fc) was added as the internal standard in the oxidation step: scan rate 100 mV/s, $TBAPF_6$ as supporting electrolyte. A and B label the first and second reduction peaks, and the corresponding reoxidation peak of A is labeled as A′. C marks the oxidation peak correlated to reoxidation of B. D and E label the first oxidation peak and its corresponding rereduction peak, respectively. The circle and asterisk mark the unidentified reduction peaks which seem sensitive to the scan region. Note that the oxidation peak of Fc is exactly overlapped with peak D. The dotted vertical lines mark the redox potentials of $TiSc_2N@C_{80}$ reported in our previous papers (refs 16 and 17).

which includes also the redox potentials of $TiSc_2N@C_{80}$ for comparison (see also Figure S5, Supporting Information, for the detailed comparison). The characteristic potentials are summarized in Table 2. In the anodic region, $TiY_2N@C_{80}$ exhibits one reversible oxidation step with a half-wave potential ($E_{1/2}$) at 0.00 V, which is more negative than that of $TiSc_2N@C_{80}$ (0.16 V).[16,17] On the other hand, the reduction steps show a complex behavior with several distinct steps. The first reduction step was evidently reversible with $E_{1/2}$ observed at −1.11 V, which is again more negative than that of $TiSc_2N@C_{80}$ (−0.94 V).[16,17] However, the second step is obviously irreversible with peak potentials (E_p) at −1.79 V. The redox behavior of $TiY_2N@C_{80}$ is dramatically different from that of $TiSc_2N@C_{80}$, which shows three reversible reduction steps (see Figure 7 and Figure S5, Supporting Information),[16,17] indicating the strong influence of the encaged group-III metal (Y or Sc) on the electronic property of these two Ti-based MMNCFs $TiM_2N@C_{80}$ (M = Y, Sc).

For $TiSc_2N@C_{80}$, our previous study pointed out that the reversible behavior in both reduction and oxidation steps was completely different than $Sc_3N@C_{80}$, and the first oxidation and reduction of $TiSc_2N@C_{80}$ occurred at the endohedral cluster, changing the valence state of Ti from Ti(II) in the anion to Ti(III) in the neutral state and to Ti(IV) in the cation.[16,17] For $TiY_2N@C_{80}$, the similar reversibilities of both the first reduction and the first oxidation steps enable us to

dx.doi.org/10.1021/ic202354u | Inorg. Chem. 2012, 51, 3039–3045

Table 2. Redox Potentials (V vs Fc/Fc^+) and Electrochemical Energy Gaps ($\Delta E_{gap,ec}$) of $TiY_2N@C_{80}$, $Sc_2TiN@C_{80}$, and $Y_3N@C_{80}$

	$E_{1/2}$ (V vs Fc/Fc^+)				
	reduction steps (E_{red})				
samples	first	second	third	oxidation step (E_{ox})	$\Delta E_{gap,ec}$/V[a]
$TiY_2N@C_{80}$	−1.11	−1.79 (E_p)[b]		0.00	1.11
$TiSc_2N@C_{80}$[16,17]	−0.94	−1.58	−2.21	0.16	1.10
$Y_3N@C_{80}$ (I_h)[1d]	−1.41 (E_p)[b]	−1.83 (E_p)[b]		0.64	2.05

[a] $\Delta E_{gap,ec} = E_{1/2,ox(1)} - E_{1/2,red(1)}$. [b] E_p: peak potential.

draw a similar conclusion that the valence state of Ti within $TiY_2N@C_{80}$ changes from Ti(III) (in the neutral state) to Ti(II) (in the anion) and to Ti(IV) (in the cation) during the first oxidation and reduction steps, respectively. This conclusion is solidified by the result that the electrochemical energy gap ($\Delta E_{gap,ec}$) of $TiY_2N@C_{80}$ (1.11 V) is almost the same as that of $Sc_2TiN@C_{80}$ (1.10 V)[16,17] despite the negative shifts of both the oxidation and the reduction potentials of $TiY_2N@C_{80}$ (see Table 2). Thus, $TiY_2N@C_{80}$ respresents a new example of endohedral fullerenes exhibiting endohedral redox behavior.[24]

The redox behavior of $TiY_2N@C_{80}$ is found to be completely different from that of $Y_3N@C_{80}$ (I_h) in terms of the reversibility of the reduction steps, the redox potentials, and $\Delta E_{gap,ec}$.[1d,25] For $Y_3N@C_{80}$ (I_h), two irreversible reduction steps with peak potentials (E_p) at −1.41 and −1.83 V and one reversible oxidation step with $E_{1/2}$ at 0.64 V were reported (see Table 2).[1d] The plausible explanation of the irreversible reductions steps of $Y_3N@C_{80}$ (I_h) is the facile dimerization of its anion radical.[26] On the contrary, the anion of $TiY_2N@C_{80}$ is expected to be diamagnetic and hence not prone to dimerization. Noteworthy, $\Delta E_{gap,ec}$ of $TiY_2N@C_{80}$ (1.11 V) is dramatically smaller than that of $Y_3N@C_{80}$ (I_h, 2.05 V),[1d] while their difference on the optical band gap obtained from UV−vis−NIR measurement as discussed above (1.39 eV for $TiY_2N@C_{80}$ vs 1.58 eV for $Y_3N@C_{80}$ (I_h)) is much smaller. A plausible explanation to the difference in $\Delta E_{gap,ec}$ between $TiY_2N@C_{80}$ and $Y_3N@C_{80}$ (I_h) is that $\Delta E_{gap,ec}$ of $TiY_2N@C_{80}$ corresponds to the reduction/oxidation of the encaged Ti atom, whereas for $Y_3N@C_{80}$ (I_h) it corresponds to reduction/oxidation of the C_{80} carbon cage.[1d,26]

CONCLUSIONS

In summary, we successfully synthesized, isolated, and characterized $TiY_2N@C_{80}$ as the first Ti-containing non-Sc MMNCF, which is compared with $TiSc_2N@C_{80}$ so as to study the influence of the group-III metal. $TiY_2N@C_{80}$ was isolated by multistep HPLC, revealing that the elution behavior of Ti-containing MMNCFs $TiM_2N@C_{80}$ (M = Y, Sc) is not a simple size effect but dependent on the nature of the group-III metal. UV−vis−NIR spectroscopic characterization of $TiY_2N@C_{80}$ indicates that the optical band gap of $TiY_2N@C_{80}$ (1.39 eV) is quite close to that of $TiSc_2N@C_{80}$ (1.43 eV) but much smaller than that of $Y_3N@C_{80}$ (I, I_h, 1.58 eV). The UV−vis−NIR spectrum of $TiY_2N@C_{80}$ shows a higher resemblance to that of $TiSc_2N@C_{80}$, both exhibiting broad shoulder absorptions. XPS study suggests that the valence state of Ti within $TiY_2N@C_{80}$ is 3; thus, the electronic configuration of $(TiY_2N)^{6+}@C_{80}^{6-}$ is proposed, which is confirmed by ESR characterization. FTIR spectroscopic study and DFT computations lead to the assignment of the C_{80}:I_h isomer to the cage structure of $TiY_2N@C_{80}$ with the C_1 conformer being the lowest energy structure, which is different from the C_s conformer assigned to $TiSc_2N@C_{80}$. These results suggest that the cage isomeric structure of $TiM_2N@C_{80}$ (M = Y, Sc) is sensitively dependent on the encaged group-III metal.

The cyclic voltammetric study of $TiY_2N@C_{80}$ reveals one reversible oxidation step with $E_{1/2}$ at 0.00 V and a reversible first reduction step with $E_{1/2}$ at −1.11 V. Although both the first oxidation and the first reduction steps are obviously more negative than those of $TiSc_2N@C_{80}$, $\Delta E_{gap,ec}$ of $TiY_2N@C_{80}$ (1.11 V) is almost the same as that of $TiSc_2N@C_{80}$ (1.10 V). On the basis of these results, we propose that, similar to the case of $TiSc_2N@C_{80}$, the valence state of Ti within $TiY_2N@C_{80}$ changes from Ti(III) (in the neutral state) to Ti(II) (in the anion) and to Ti(IV) (in the cation) during the first oxidation and first reduction steps. However, the second reduction steps of $TiY_2N@C_{80}$ are obviously irreversible with E_p at −1.79 V, and this redox behavior is dramatically different from $TiSc_2N@C_{80}$, which shows three reversible reduction steps instead, indicating the strong influence of the encaged group-III metal (Y or Sc) on the electronic property of $TiM_2N@C_{80}$ (M = Y, Sc). On the basis of the above comparative studies on the yield, elution behavior, redox property, and most stable conformer structure between $TiY_2N@C_{80}$ and $TiSc_2N@C_{80}$, the strong influence of the group-III metal on the structure and properties of $TiM_2N@C_{80}$ (M = Y, Sc) is revealed. This study provides new insight into the metal nitride clusterfullerenes and would stimulate the synthesis of novel endohedral fullerenes.

EXPERIMENTAL SECTION

$TiY_2N@C_{80}$ was synthesized in a modified Krätschmer−Huffman generator by vaporizing composite graphite rods (Φ 8 × 150 mm) containing a mixture Y_2O_3, TiO_2, and graphite powder (molar ratio = 1:1:30) with addition of N_2 (10 mbar) into 400 mbar He. The soot was collected and Soxhlet extracted by CS_2 for 24 h. Then CS_2 was removed, and the extract was immediately redissolved in toluene (~ 200 mL) and subsequently passed through a 0.2 μm Telflon filter (Sartorius AG, Germany) for HPLC separation. The purity of the isolated products was checked by laser desorption time-of-flight (LD-TOF) MS analysis (Biflex III, Bruker, Germany) running in both positive- and negative-ion modes. UV−vis−NIR spectra of fullerenes were performed on a UV−vis−NIR 3600 spectrometer (Shimadzu, Japan) using a quartz cell of 1 mm layer thickness and 1 nm resolution. For FTIR measurement of $TiY_2N@C_{80}$, the sample was drop coated onto KBr single-crystal disks. The residual toluene was removed by heating the polycrystalline films in a vacuum of 2×10^{-6} mbar at 235 °C for 3 h. The FTIR spectrum was recorded at room temperature on an IFS 66v spectrometer (Bruker, Germany). For XPS measurements, thin films of $TiY_2N@C_{80}$ drop coated onto KBr single-crystal disks were transferred under ultrahigh vacuum conditions into an ESCALAB 250 spectrometer (Thermo-VG Scientific, England) using monochromatic Al Kα radiation (1486.6 eV) with an energy resolution of 0.6 eV. ESR spectra of $TiY_2N@C_{80}$ were measured in toluene solution using a JES-FA200 FT-EPR X-band spectrometer (JEOL, Japan).

dx.doi.org/10.1021/ic202354u | Inorg. Chem. 2012, 51, 3039−3045

Electrochemical study of $TiY_2N@C_{80}$ was performed in *o*-dichlorobenzene (*o*-DCB, anhydrous, 99%, Aldrich). The supporting electrolyte was tetrabutylamonium hexafluorophosphate ($TBAPF_6$, puriss. electrochemical grade, Fluka) which was dried under pressure at 340 K for 24 h and stored in a glovebox prior to use. Cyclic voltammogram experiments were performed with a CHI 660 potentiostat (CHI Instrument, USA) at room temperature in a glovebox. A standard three-electrode arrangement of a platinum (Pt) wire as the working electrode, a platinum coil as the counter electrode, and a silver wire as a pseudoreference electrode was used. In a comparison experiment, ferrocene (Fc) was added as the internal standard and all potentials are referred to the Fc/Fc^+ couple.

Details of Computations. Our calculations are performed using density functional theory (DFT)[27] as implemented in the DMol[3] package[28] based on the linear combination of the atomic orbital−molecular orbital. The atomic orbitals are represented by a double-numeric quality basis set with polarization functions (DNP), which are comparable to Gaussian 6-31G** sets. The exchange correlation interactions are described by the Perdew−Burke−Ernzerhof generalized gradient approximation (GGA).[29] All atomic positions are fully relaxed at the GGA level without symmetry restriction until the atomic forces are smaller than 10^{-5} Hartree. The electronic structure is obtained by solving the Kohn−Sham equations self-consistently in the spin-polarized scheme, and the self-consistent field procedure is carried out with a convergence criterion of 10^{-6} Hartree on the energy and electron density.

■ ASSOCIATED CONTENT

Supporting Information

LD-TOF MS spectra of fraction **A**, isolation of $TiY_2N@C_{80}$ and estimation of the relative yield of $TiY_2N@C_{80}$ to that of $Y_3N@C_{80}$ (I), XPS spectra of $TiY_2N@C_{80}$, and comparison of cyclic voltammograms of $TiY_2N@C_{80}$ and $TiSc_2N@C_{80}$. This material is available free of charge via the Internet at http://pubs.acs.org.

■ AUTHOR INFORMATION

Corresponding Author

*E-mail: sfyang@ustc.edu.cn.

■ ACKNOWLEDGMENTS

We are grateful to valuable discussions with Professors Alan L. Balch and Marilyn M. Olmstead and Miss Faye Bowles (University of California—Davis), Professor Sergey I. Troyanov (Moscow State University), and Professor Jihu Su (University of Science and Technology of China). This work was supported by grants from the National Natural Science Foundation of China (20801052, 90921013, 11074235, 11034006), "100 Talents Programme" of CAS, the Scientific Research Foundation for the Returned Overseas Chinese Scholars of MOE ([2010]609), and the National Basic Research Program of China (2010CB923300, 2011CB921400). A.P. acknowledges financial support from DFG.

■ REFERENCES

(1) For recent reviews, see (a) Dunsch, L.; Yang, S. F. *Small* **2007**, *3*, 1298−1320. (b) Dunsch, L.; Yang, S. F. *Phys. Chem. Chem. Phys.* **2007**, *9*, 3067−3081. (c) Yang, S. F.; Dunsch, L. Endohedral Fullerenes. *Nanomaterials: Inorganic and Bioinorganic Perspectives*; Lukehart, C. M., Scott, R. A., Eds.;John Wiley & Sons, Ltd.: Chichester, U.K., 2008; pp 189−214. (d) Chaur, M. N.; Melin, F.; Ortiz, A. L.; Echegoyen, L. *Angew. Chem., Int. Ed.* **2009**, *48*, 7514−7538. (e) Rodríguez-Fortea, A.; Balch, A. L.; Poblet, J. M. *Chem. Soc. Rev.* **2011**, *40*, 3551−3563. (f) Yang, S. F.; Liu, F. P.; Chen, C. B.; Jiao, M. Z.; Wei, T. *Chem. Commun.* **2011**, *47*, 11822−11839.

(2) Stevenson, S.; Rice, G.; Glass, T.; Harich, K.; Cromer, F.; Jordan, M. R.; Craft, J.; Hadju, E.; Bible, R.; Olmstead, M. M.; Maitra, K.; Fisher, A. J.; Balch, A. L.; Dorn, H. C. *Nature* **1999**, *401*, 55−57.

(3) Dunsch, L.; Krause, M.; Noack, J.; Georgi, P. *J. Phys. Chem. Solids* **2004**, *65*, 309−315.

(4) Yang, S. F.; Liu, F. P.; Chen, C. B.; Zhang, W. F. *Prog. Chem.* **2010**, *22*, 1869−1881.

(5) Chen, N.; Zhang, E. Y.; Wang, C. R. *J. Phys. Chem. B* **2006**, *110*, 13322−13325.

(6) Wang, X. L.; Zuo, T. M.; Olmstead, M. M.; Duchamp, J. C.; Glass, T. E.; Cromer, F.; Balch, A. L.; Dorn, H. C. *J. Am. Chem. Soc.* **2006**, *128*, 8884−8889.

(7) Yang, S. F.; Popov, A. A.; Chen, C. B.; Dunsch, L. *J. Phys. Chem. C* **2009**, *113*, 7616−7623.

(8) Yang, S. F.; Kalbac, M.; Popov, A. A.; Dunsch, L. *ChemPhysChem* **2006**, *7*, 1990−1995.

(9) Yang, S. F.; Popov, A. A.; Kalbac, M.; Dunsch, L. *Chem.—Eur. J.* **2008**, *14*, 2084−2092.

(10) Stevenson, S.; Chancellor, C. J.; Lee, H. M.; Olmstead, M. M.; Balch, A. L. *Inorg. Chem.* **2008**, *47*, 1420−1427.

(11) Yang, S. F.; Popov, A. A.; Dunsch, L. *J. Phys. Chem. B* **2007**, *111*, 13659−13663.

(12) Olmstead, M. M.; de Bettencourt-Dias, A.; Duchamp, J. C.; Stevenson, S.; Dorn, H. C.; Balch, A. L. *J. Am. Chem. Soc.* **2000**, *122*, 12220−12226.

(13) Yang, S. F.; Popov, A. A.; Dunsch, L. *Chem. Commun.* **2008**, 2885−2887.

(14) Yang, S. F.; Popov, A. A.; Dunsch, L. *Angew. Chem., Int. Ed.* **2008**, *47*, 8196−8200.

(15) Zhang, L.; Popov, A. A.; Yang, S. F.; Klod, S.; Rapta, P.; Dunsch, L. *Phys. Chem. Chem. Phys.* **2010**, *12*, 7840−7847.

(16) Yang, S. F.; Chen, C. B.; Popov, A. A.; Zhang, W. F.; Liu, F. P.; Dunsch, L. *Chem. Commun.* **2009**, 6391−6393.

(17) Popov, A. A.; Chen, C. B.; Yang, S. F.; Lipps, F.; Dunsch, L. *ACS Nano* **2010**, *4*, 4857−4871.

(18) Greenwood, N. N.; Earnshaw, A. *Chemistry of the Elements*; Pergamon: Oxford, 1984.

(19) Yang, S. F.; Troyanov, S. I.; Popov, A.; Krause, M.; Dunsch, L. *J. Am. Chem. Soc.* **2006**, *128*, 16733−16739.

(20) Li, S. J.; Lei, S. L.; Huang, J.; Li, Q. X. *Chin. J. Chem. Phys.* **2011**, *24*, 439−443.

(21) Because DFT calculations revealed that the conformers of TiSc2N@C_{80}-D_{5h} are at least 56 kJ·mol^{-1} less stable than those of the I_h-based conformers, only conformers based on $TiSc_2N@C_{80}$-I_h are discussed.

(22) Echegoyen, L.; Chancellor, C. J.; Cardona, C. M.; Elliott, B.; Rivera, J.; Olmstead, M. M.; Balch, A. L. *Chem. Commun.* **2006**, 2653−2655.

(23) Lukoyanova, O.; Cardona, C. M.; Rivera, J.; Lugo-Morales, L. Z.; Chancellor, C. J.; Olmstead, M. M.; Rodriguez-Fortea, A.; Poblet, J. M.; Balch, A. L.; Echegoyen, L. *J. Am. Chem. Soc.* **2007**, *129*, 10423−10430.

(24) Popov, A. A.; Dunsch, L. *J. Phys. Chem. Lett.* **2011**, *2*, 786−794.

(25) Tarábek, J.; Yang, S. F.; Dunsch, L. *ChemPhysChem* **2009**, *10*, 1037−1043.

(26) Popov, A. A.; Avdoshenko, S. M.; Cuniberti, G.; Dunsch, L. *J. Phys. Chem. Lett.* **2011**, *2*, 1592−1600.

(27) Kohn, W.; Sham, L. J. *Phys. Rev.* **1965**, *140*, A1133−A1138.

(28) Delley, B. *J. Chem. Phys.* **1990**, *92*, 508−517.

(29) Perdew, J. P.; Burke, K.; Ernzerhof, M. *Phys. Rev. Lett.* **1996**, *77*, 3865−3868.